Circuit Characterization of *V*-Band IMPATT Oscillators and Amplifiers

T. T. FONG, MEMBER, IEEE, KENNETH P. WELLER, MEMBER, IEEE, AND DAVID L. ENGLISH, ASSOCIATE MEMBER, IEEE

Abstract—**A circuit model has been developed to describe a class of commonly used waveguide cavities for *V*-band IMPATT oscillators and amplifiers. Calculated results based on this model used in conjunction with theoretical small-signal IMPATT characteristics have shown good qualitative agreement with experimental data. Detailed characterization of a small-signal *V*-band IMPATT amplifier and a mechanical tuned oscillator are presented, and the predicted performance is compared with measurements.**

I. Introduction

UNTIL RECENTLY, the design of IMPATT components for millimeter-wave applications has relied heavily on the "cut-and-try" approach with some intuitive guidance. An analytical design approach is not widely used mainly because of the difficulty encountered in obtaining an accurate model to describe the circuit. This paper presents an effort made toward designing active millimeter-wave components utilizing a circuit model in conjunction with the small-signal IMPATT characteristics. Although the model developed contains gross approximations resulting from a compromise between mathematical rigor and practical application of the model without excessive numerical calculation, the results show good agreement with experiments. The purpose of this paper is therefore not to cast a precise model for millimeter-wave IMPATT circuits, which is exceedingly complex and difficult, but to summarize a design approach that provides qualitative predictions to aid in circuit design.

II. Circuit Modeling

The basic circuit under consideration is a reduced-height waveguide circuit in which a packaged diode is mounted under a round metallic bias post with a movable short provided behind the post for tuning. A short-circuited coaxial section is provided in the top waveguide wall for impedance matching. A cross section of the circuit is shown in Fig. 1. This circuit configuration has been widely used as an IMPATT cavity [1], [2] and has been studied in the past [3]–[7]. However, the mathematical complexity has prevented the development of a concise model that can be used efficiently for circuit design over a wide range of circuit parameters. Approximations are generally used to simplify the analysis. The resulting equivalent circuit model is therefore valid only for a range of parameters. Our experience has shown that a circuit model which applies well at lower microwave frequencies is often inadequate for commonly used millimeter-wave circuit parameters.

Manuscript received February 6, 1976; revised May 10, 1976.
The authors are with the Torrance Research Center, Hughes Aircraft Company, Torrance, CA 90509.

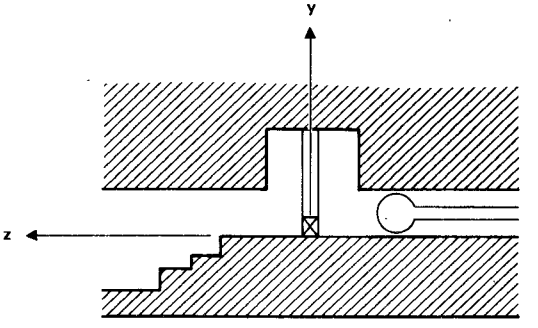

Fig. 1. A reduced-height waveguide IMPATT circuit with a cross-coupled coaxial section above the diode.

In order to develop an adequate model for millimeter-wave circuits, two specific considerations are in order. 1) In many applications the diameter of the bias post is relatively large in terms of the waveguide width (i.e., $d/a > 0.2$ in Fig. 2), which makes the commonly used thin post approximation rather inaccurate. 2) In active millimeter component development, the tuning short is often positioned in close proximity to the bias post to achieve proper operation. In this case the higher order waveguide modes may not be sufficiently attenuated to neglect the interaction between the post and the tuning short. These factors will significantly modify the current distribution on the post resulting in reactance change. In this paper we will attempt to develop a first-order circuit model incorporating these two elements.

To accurately account for the diode mounting parasitics, the driving point impedance of a post with a gap must be considered. Lewin [6] has derived an approximate equivalent circuit for a thin post containing a gap at the waveguide floor. Although his analysis results in a diverging series because of certain assumptions made, the equivalent circuit derived deals with a broad class of waveguide circuits with explicit physical interpretation on the circuit elements, and makes it attractive for circuit design. Eisenhart and Kahn [7], through the use of dyadic Green's function, have derived the driving point impedance of a flat post with arbitrary gap width and position. Later, Bradshaw [8] formulated a general analysis which considers a thin round post. For millimeter-wave applications, a precise equivalent circuit requires the detailed consideration of a large diameter post containing a gap, which poses a formidable mathematical problem. The solution of such a problem will likely involve extensive use of numerical techniques, which limits its usefulness. For the purpose of achieving qualitative design guidelines, we will seek an approximate model

to allow rapid circuit design. Our approach to the development of an equivalent circuit model for the cavity (shown in Fig. 1) can be outlined in two steps.

1) Firstly, the analysis of a large diameter post, with no gap, extending across a reduced-height waveguide in close proximity to the short is considered. We attempt to derive the post reactance taking into consideration the large diameter post as well as the interaction between the post and the short through higher order modes. The post current distribution in the y direction (Fig. 1) is assumed to be a constant, which is a valid approximation for reduced-height waveguide.

2) Secondly, a gap under the post and a cross-coupled coaxial section above the post are included in an approximate manner.

The current distribution on the post in the transverse y direction, caused by a gap at the bottom of the post (Fig. 1), can be represented by a Fourier expansion:

$$I(y) = I_o + \sum_{n=1}^{\infty} \left[A_n \cos\left(\frac{n\pi y}{b}\right) + B_n \sin\left(\frac{n\pi y}{b}\right) \right] = I_o + \Delta(y) \quad (1)$$

where b is the waveguide height.

Assuming that the current distribution is a slowly varying function in y for a short post (reduced-height waveguide), the higher order Fourier components constitute a minor modification to the dominating constant current component. Therefore, we assume that the modifications due to the higher order current components can be made according to the analysis by Lewin [6]. Furthermore, following Lewin, the top coaxial section (Fig. 1) is modeled by a gap terminated by the input impedance of the coaxial section [6]. This approach leads to an equivalent circuit model for the cavity shown in Fig. 1. Our procedure for including the gap parasitics and the coaxial section impedance is done without analytical rigor to simplify the analysis. However, the agreement between experimental oscillator and amplifier behavior and the equivalent circuit model prediction is good enough to make the model a useful design tool.

The analysis of the large diameter post in a reduced-height waveguide proceeds by assuming a constant post current distribution in y. The assumption of a constant current distribution in y simplifies the boundary value problem to a two-dimensional scalar field problem, and the solution can be found in a straightforward manner. Since the analysis is quite standard and the essentials can be found in many textbooks [9]–[11], only the key steps will be outlined here.

The coordinate system for the problem to be solved is shown in Fig. 2. The characteristic Green's function G satisfies the inhomogeneous wave equation

$$\left(\frac{\partial^2}{\partial x^2} + \frac{\partial^2}{\partial z^2} + k^2\right) G(x,z;x'z') = \delta(x - x')\delta(z - z') \quad (2)$$

where $k = \omega\sqrt{\mu_0\varepsilon_0}$. Applying the appropriate boundary conditions, the Green's function arising from a current

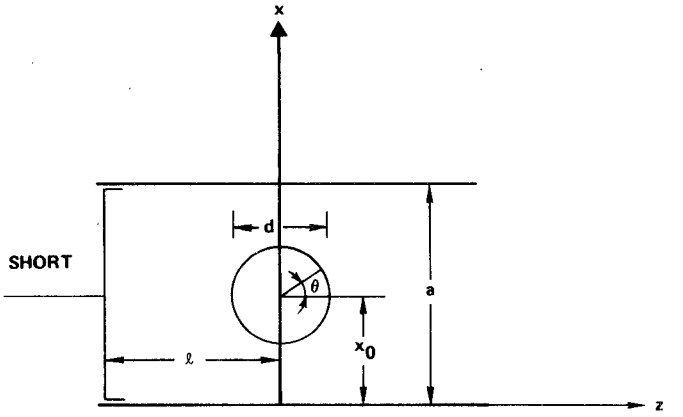

Fig. 2. Coordinate system for analysis of a waveguide with a post and an adjustable short.

filament located at (x',z') is found and

$$G(x,z;x',z') = -j \sum_{m=1}^{\infty} \frac{\sin\frac{m\pi x}{a} \sin\frac{m\pi x'}{a}}{\beta_m a} \times \left(e^{-j\beta_m|z-z'|} - e^{-j\beta_m|z+z'+2l|}\right) \quad (3)$$

where $\beta_m = [k^2 - (m\pi/a)^2]^{1/2}$. Based on (3), one can formulate an integral equation to solve for the current distribution on the post surface. In order to derive an equivalent network for the present structure, the approach developed by Schwinger and Saxon [9] using variational principles will be followed. Since the analysis is lengthy and the details are given in [9], we will only outline the results here. Considering the even and odd excitations, the equivalent network of the post can be represented by a T network; and for the even and odd incident waves

$$\psi_e(x,z) = \sin\frac{\pi x}{a} \cos\beta_1(z + l)$$

$$\psi_o(x,z) = \sin\frac{\pi x}{a} \sin\beta_1(z + l)$$

the elements of the T network can be represented by the following variational expressions:

$$Z_{11} + Z_{12} = \frac{j\beta_1 a}{2} \frac{\iint I_e(x,z)G_e(x,z;x',z')I_e(x',z')\,ds\,ds'}{\int I_e(x,z)\psi_e(x,z)\,ds} \quad (4)$$

$$\frac{1}{Z_{11} - Z_{12}} = \frac{j\beta_1 a}{2} \frac{\iint I_o(x,z)G_o(x,z;x',z')I_o(x',z')\,ds\,ds'}{\int I_o(x,z)\psi_o(x,z)\,ds}. \quad (5)$$

The integrals extend over the entire post surface. G_e and G_o are the even and odd Green's function defined by

$$G_e = G(x,z;x',z') + G(x,z;x',-z')$$

$$G_o = G(x,z;x',z') - G(x,z;x',-z')$$

and I_e and I_o are the kernels related to the current distribution on the post caused by the even and odd excitation, respectively. Expanding I_e and I_o into Fourier series and retaining only the lowest order terms, the integrals in (4)

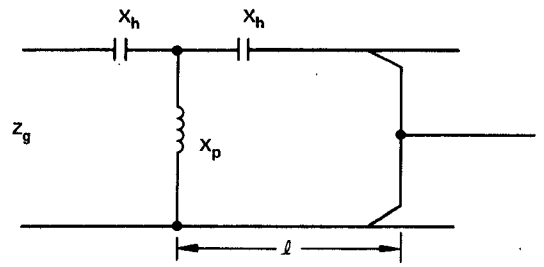

Fig. 3. Equivalent T network of a post in waveguide.

and (5) can be evaluated. It can be shown that $Z_{11} - Z_{12}$ is a capacitive reactance reflecting the average phase change from $z = \pm d$ to the center of the post, and Z_{12} is simply the post reactance. The resulting equivalent network can be represented by lumped capacitive reactance ($X_h = Z_{11} - Z_{12}$) and inductive reactance ($X_p = Z_{12}$) as shown in Fig. 3. The expressions for these reactances are

$$\frac{X_h}{Z_g} = j\,\frac{8\beta_1 a}{(ka)^2}\,\frac{J_1\left(\frac{\pi d}{\lambda}\right)}{Y_1\left(\frac{\pi d}{\lambda}\right)}\sin^2\frac{\pi x_0}{a} \tag{6}$$

$$\begin{aligned}\frac{X_p}{Z_g} = {} & j\,\frac{\beta_1 a}{4\pi}\csc^2\left(\frac{\pi x_0}{a}\right)\left\{\ln\left(\frac{4a}{\pi d}\sin\frac{\pi x_0}{a}\right) - 2\sin^2\left(\frac{\pi x_0}{a}\right)\right. \\ & \left. + \frac{1}{4}\,Y_0\left(\frac{\pi d}{\lambda}\right)\left[1 - \frac{1}{J_0\left(\frac{\pi d}{\lambda}\right)}\right] + 2S_A\right\} \\ & - j\,\frac{\beta_1 a}{4\pi}\csc^2\left(\frac{\pi x_0}{a}\right) \\ & \cdot \left\{\frac{1}{2}\ln\left[\frac{\cosh\frac{2\pi l}{a} - \cos\frac{\pi}{2a}(4x_0 + d)}{\cosh\frac{2\pi l}{a} - \cos\frac{\pi d}{2a}}\right]\right. \\ & - 2e^{-(2\pi l/a)}\sin^2\frac{\pi x_0}{a} + \frac{1}{4}\,Y_0\left(\frac{\pi d}{\lambda}\right) \\ & \left. \cdot \left[1 - \frac{1}{J_0\left(\frac{\pi d}{\lambda}\right)}\right]e^{-(2\pi l/a)} + 2S_B\right\}\end{aligned} \tag{7}$$

where

$$S_A = \sum_{m=2}^{\infty}\left(\frac{\pi}{\Gamma_m a} - \frac{1}{m}\right)\sin^2\frac{m\pi x_0}{a}$$

$$S_B = \sum_{m=2}^{\infty}\left(\frac{e^{-2\Gamma_m l}\pi}{\Gamma_m a} - \frac{e^{-(2m\pi l/a)}}{m}\right)\sin^2\frac{m\pi x_0}{a}$$

$$\Gamma_m = \left[\left(\frac{m\pi}{a}\right)^2 - k^2\right]^{1/2}$$

and $Z_g = 754((kb)/(\beta_1 a))$ is the waveguide impedance for TE_{10} mode. J and Y are the Bessel and Neumann functions, respectively. The post reactance as shown in (7) consists of two components; the first part is the self-inductance of the post, the second part can be regarded as the mutual inductance arising from the perturbation of current distribution caused by the short. This contribution is a rapidly decaying function of l, the distance between the short and the post.

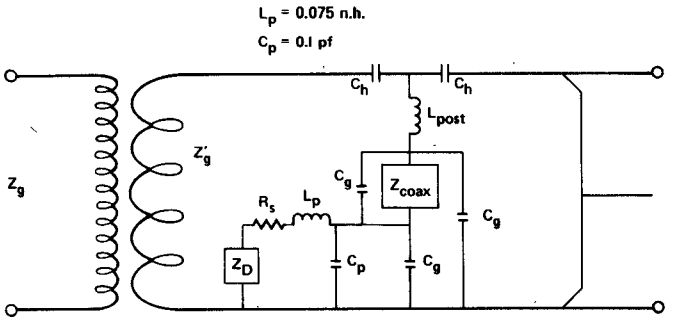

Fig. 4. Equivalent circuit model for the waveguide circuit shown in Fig. 1.

If a small gap is opened at the bottom of the post to allow mounting of the device with impedance Z, the current on the post will change as well as the field around the post. For a reduced-height waveguide, we assume that this change is small and the analysis made by Lewin [6] is approximately valid for our case. The parasitics caused by the gap as derived by Lewin can therefore be integrated with the equivalent circuit shown in Fig. 3 to complete our circuit model. Furthermore, the gap terminated by an impedance Z can also be approximated by a coaxial section [6] having the same input impedance, provided that no higher order modes propagate in the coax. The circuit configuration is shown in Fig. 1, and its approximate equivalent circuit model is shown in Fig. 4. Z_{coax} is the input impedance of the coaxial section and C_g and C_g' are the post mounting gap parasitics. The expressions for C_g and C_g' are [6]

$$\omega C_g = \frac{kb}{30\pi^2\ln\left(\frac{4a}{\pi d}\right)}\sum_{m=1}^{\infty}\frac{(1 - \cos m\pi)\xi}{m^2 - \left(\frac{kb}{\pi}\right)^2} \tag{8}$$

$$\omega C_g' = \frac{kb}{30\pi^2\ln\left(\frac{4a}{\pi d}\right)}\sum_{m=1}^{\infty}\frac{(\cos m\pi)\xi}{m^2 - \left(\frac{kb}{\pi}\right)^2} \tag{9}$$

where

$$\xi = \frac{e^{-m\pi d/2b}\ln\left(\frac{4a}{\pi d}\sin\frac{\pi x_0}{a}\right)}{K_0\left(\frac{m\pi d}{2b}\right) - K_0\left(\frac{2m\pi x_0}{b}\right)}$$

and K_0 is the modified Bessel function of the second kind. It is of particular interest to note that, though C_g' has the frequency dependence of a capacitance, its reactance has a positive sign. This gives rise to some interesting effects, and an example will be discussed in a following section.

Also shown in Fig. 4 are the diode package parasitics. In our case, the millimeter-wave IMPATT diode is mounted in a quartz ring package which consists of a connection gold ribbon (0.001 by 0.003 in), and a quartz ring (0.030-in

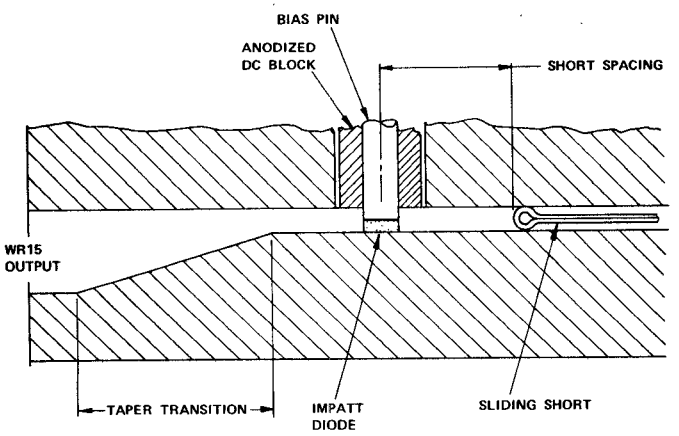

Fig. 5. Reduced-height waveguide circuit with packaged diode mounted under the post.

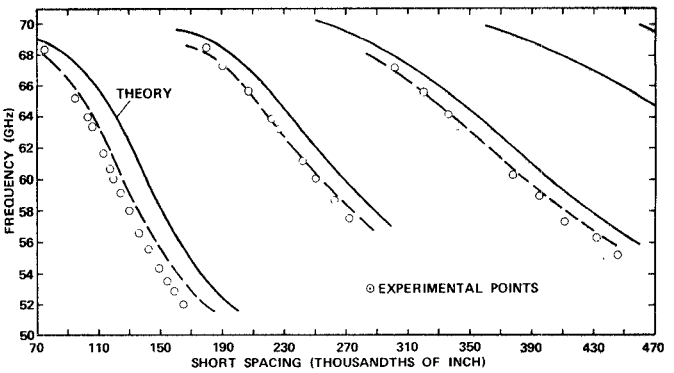

Fig. 6. Calculated and measured mechanical tuning behavior for the IMPATT oscillator shown in Fig. 5.

outer diameter, 0.020-in inner diameter, and 0.005-in in height). The package parasitics are modeled by an ideal inductance (L_p) in series with the diode and an ideal capacitance (C_p) in shunt with the inductance. Their values have been determined initially by means of low-frequency measurements at 10 GHz using a network analyzer, and confirmed at V band by means of DeLoach measurements [12]. The values so determined are $L_p = 0.075$ nH and $C_p = 0.1$ pF. These values can only be considered typical since there is some scatter in the parameters from package to package.

III. Oscillator Characterization

Using a simple reduced-height waveguide circuit as shown schematically in Fig. 5, which is a special case ($Z_{coax} = 0$) of the circuit shown in Fig. 1, an extensive set of oscillator data have been taken for comparison with the computer simulation based on the circuit model discussed previously. This exercise was performed to gain confidence in the model and demonstrate the bandwidth prediction capabilities. The experimental circuit used has a reduced-height section of 0.020-in height with a taper transition to full-height WR15 waveguide at the output. The spring contacting sliding short in the reduced-height section is driven by a micrometer to accurately determine its position during the measurements.

The diode used for the experiment is an n-type flat-profile single-drift diode with doping density of 1×10^{17} cm^{-3}. The device has a junction area of 1.5×10^{-5} cm^2 and was biased to a current density of 19.4 kA/cm^2. For the purpose of the computer simulation, these parameters were determined carefully using standard capacitance–voltage measurement techniques. The power and frequency of the IMPATT oscillator has been determined as a function of short position over a wide mechanical tuning range. The frequency data are plotted in Fig. 6. Here the frequency of oscillation is plotted as a function of the spacing between the center line of the IMPATT bias post and the front edge of the sliding short.

The solid theoretical curves shown in Fig. 6 were obtained by means of the equivalent circuit model developed in Section II in conjunction with a computer generated small-signal admittance characteristic for the IMPATT diode based on the analysis by Misawa [13]. The silicon ionization rates of Grant [14] are used in the analysis. The circuit admittance presented to the diode chip is calculated using the equivalent circuit model as shown in Fig. 4 by letting $Z_{coax} = 0$.

The point of oscillation for each short position is found by finding the frequency at which the diode susceptance cancels the circuit susceptance presented to the diode chip. In addition, for an oscillation to build up, the magnitude of the device negative conductance must be greater than the circuit conductance presented to the device. The theoretical predicted oscillation frequency versus short spacing generated in this manner are shown as solid curves in Fig. 6. The criterion used to generate these curves is only approximate since the small-signal device characteristic is being used to predict the large-signal oscillation frequency. In reality, the device susceptance increases as the RF amplitude increases, thereby making the stable point of oscillation somewhat lower in frequency than predicted by the small-signal criterion.

It is evident from Fig. 6 that there is some discrepancy in short position between the theoretical prediction (solid curve) and experimental points. Much closer agreement is obtained by shifting the theoretical curve a constant 0.015 in in short position as indicated by the dashed curve. It is as if the effective short position was 0.015 in further from the IMPATT diode than was measured experimentally. The shift can be at least partially explained by the fact that our short is not ideal. The short is curved as shown in Fig. 5, and makes contact with the broad walls of the waveguide approximately 0.010 in behind the front edge of the short from which the short spacing is referenced. In any case, this uncertainty in short position is not a serious problem since most millimeter components are provided with a tunable short for fine tuning.

The remaining discrepancy between the dashed curve and experiment can be explained on the basis of large-signal effects. In Fig. 7 the small-signal device characteristic used to generate the solid curves in Fig. 6 is shown as a function of frequency in the admittance plane. The negative of the circuit admittance presented to the diode for a short

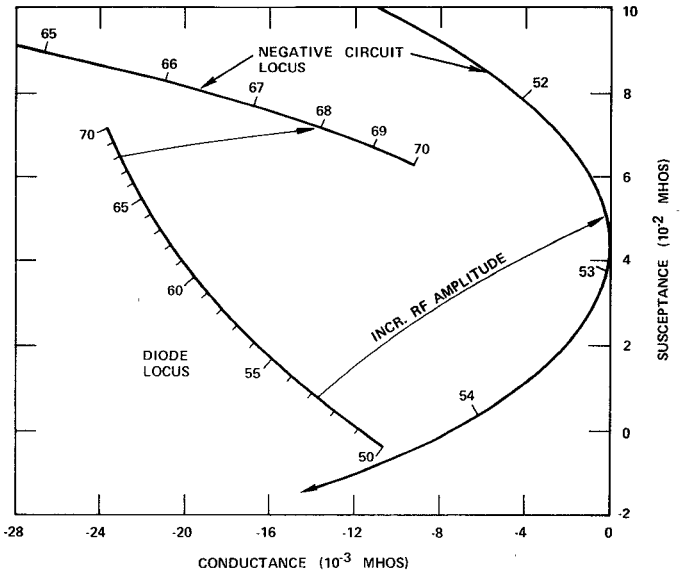

Fig. 7. Device and circuit characteristics for a short spacing of 0.180 in plotted in the admittance plane as a function of frequency in gigahertz indicated by tick marks on the curves.

spacing of 0.180 in is also shown. This short spacing was chosen for illustration because a frequency jump is predicted near this point. The downward shift in frequency due to large-signal considerations can be estimated from this figure. A qualitative estimate of the shift in the device characteristics as RF amplitude increases is indicated for the two possible stable points of oscillation indicated by the arrows. The shift in susceptance with signal level is expected to be large at the low-frequency end of the characteristic as indicated [15]. Even so, the downward shift in the stable point of oscillation from the small-signal prediction is only expected to be on the order of 1 GHz. This small shift is due to the rapid variation in circuit susceptance with frequency (high circuit Q). The circuit Q is much lower at the higher frequency point of interception, but the device susceptance increase with signal level is much smaller. Here the downward shift is estimated to be on the order of 0.5 GHz. As can be seen in Fig. 6, the tuning pattern repeats itself at multiple half-guided wavelengths. For larger short spacing, the large-signal frequency shift is expected to decrease due to increased circuit Q. These relative estimates in the downward shift in frequency due to large-signal behavior are borne out in comparing the experimental and theoretical data of Fig. 6. The discrepancy between small-signal prediction and experiment is largest for the closest tuning range of short spacing of 0.070–0.180 in, with the biggest discrepancy at the low-frequency end of the curve.

Over much of the short-spacing range, only one intersection between diode and circuit loci is possible. However, near the frequency jump points, such as is illustrated in Fig. 7, two intersections are possible. In fact, near these points, multifrequency or very noisy oscillations are often observed. As the short is moved away from the IMPATT diode, but before reaching a frequency jump point, the lower frequency intersection dominates. At the higher frequency intersection, the circuit load conductance is almost as large in magnitude as the device small-signal conductance, so a large amplitude oscillation is not possible. In fact, incidental device and circuit losses, not taken into account in the computer model, appear to have completely suppressed oscillation at the high-frequency end of the tuning curve above 68.5 GHz. As the short is moved through the frequency jump point, the circuit loading of the lower frequency intersection point becomes very small. This results in a noisy low-power output since a very large RF voltage amplitude can exist, but little power is coupled to the output. At the same time, the circuit conductance of the higher frequency intersection point is decreasing, allowing a larger amplitude oscillation and higher power output. Finally, as the short spacing is increased further, the low-frequency intersection point disappears and the high-frequency power output improves. Qualitatively, all the features of the oscillator behavior near the frequency jump point can be explained in this manner.

IV. Small-Signal Amplifier Characterization

To further test the accuracy of the circuit model as shown in Fig. 4, a small-signal IMPATT amplifier has been characterized in detail. The amplifier circuit consists of a reduced-height waveguide (0.025-in height) cross coupled to a coaxial section (0.030-in center conductor, 0.073-in outer conductor) on top of the waveguide. The coaxial section is terminated by a short. The packaged IMPATT diode is mounted under the bias post on the floor of the waveguide. A cross section of the circuit is shown in Fig. 1. The coaxial section above the diode is required to suppress oscillation and provide the desired frequency response in the amplifier. The coaxial section length is an important tuning element in the amplifier. The IMPATT diode used for the experiment is an n-type flat-profile single-drift diode with doping density of 1×10^{17} cm^{-3}. The device has a junction area of 2×10^{-5} cm^2 and was biased at a current density 17.5 kA/cm^2. The theoretical calculated small-signal admittance for this device is shown in Fig. 8.

A distinctive characteristic of this amplifier is that its gain response always consists of two peaks (double tuned). The high-frequency peak is not tunable and occurs at a fixed frequency; the low-frequency peak is tunable only by varying the coaxial length. Unlike the simple reduced-height circuit discussed in the preceding section, the short position has a negligible effect on the amplifier frequency response. It only controls the magnitude of the gain peaks; one peak is usually enhanced at the expense of the other one. It is, therefore, possible to set the gain peaks at equal magnitude simply by adjusting the short position for a given coaxial length. The unique properties of this amplifier can be explained on the bias of the equivalent circuit model shown in Fig. 4.

Since the single-drift IMPATT device has a low impedance, the matching to the waveguide must be accomplished by impedance transformation through the circuit network. In this case the transformation is achieved by means of parallel resonances. One resonance is directly

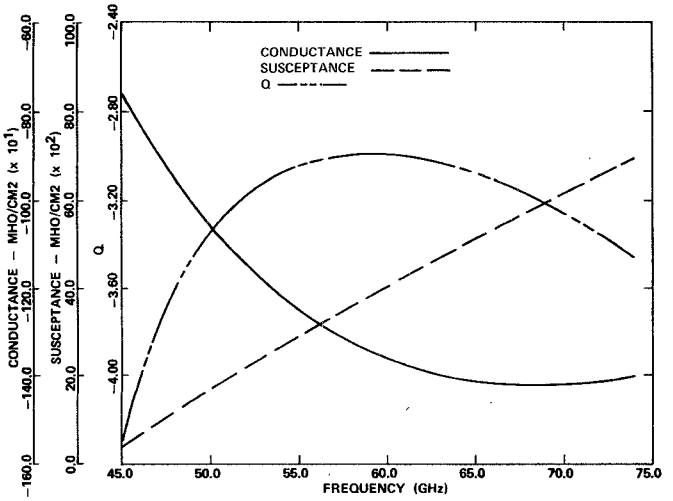

Fig. 8. Calculated small-signal IMPATT admittance as a function of frequency for a flat doping density (n-type) of 1×10^{17} cm^{-3} and a current density of 17.5 kA/cm^2.

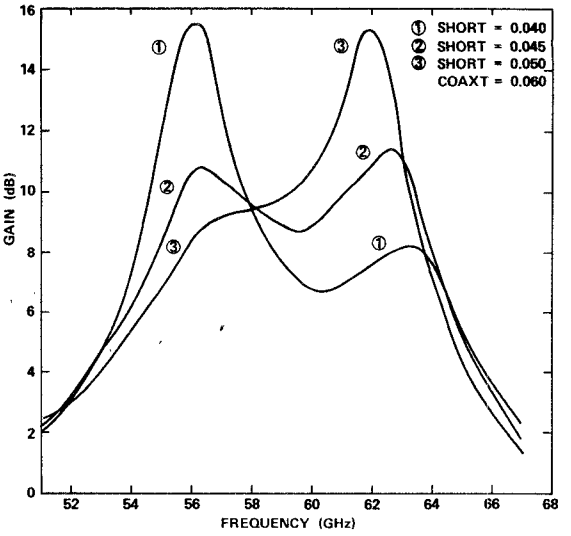

Fig. 9. Calculated amplifier gain for a fixed coaxial length as a function of short position.

attributed to the device–package parasitics. For a given device and package this resonance occurs at a fixed frequency. Furthermore, because of the relatively high Q, the resonance frequency is fairly independent of external tuning. This explains why the high-frequency response of the amplifier is not tunable. The low-frequency response of the amplifier arises through the parallel resonance caused by Z_{coax} and C_g' as shown in Fig. 4. In practice, the coaxial length corresponds approximately to one-quarter wavelength of the low-frequency gain peak, and it gives rise to a high capacitive reactance. As pointed out by Lewin [6], C_g' is a negative capacitance or is actually inductive in nature, and provides the necessary inductive reactance to resonant with Z_{coax}. Since C_g' is a small value in the present circuit, for the resonance to occur, the coaxial length must be close to a quarter-wavelength. This explains why the low-frequency response is controlled by the coaxial length.

Extensive calculations of the amplifier characteristics based on the equivalent circuit model using theoretical small-signal IMPATT admittance data have been carried out. It is found that good agreement has been obtained between calculation and measurements. However, the predicted short positions and coaxial lengths for equal gain response differ from those obtained from measurements. The discrepancy can be attributed at least in part to measurement inaccuracy. Since there was no provision provided in the circuit to indicate the precise short position and coaxial length, the measurements were made by disassembling the circuit after each RF evaluation. In view of this, the worst case of 30-percent discrepancy in short position is certainly not excessive, since only qualitative agreement is expected.

The amplifier response for a given coaxial length as a function of short position has also been calculated. One such example is shown in Fig. 9, where the calculated amplifier gain as a function of frequency is plotted for a fixed coaxial length of 0.060 in and three short positions. It is seen as the short moves closer to the bias post, the low-frequency gain peak increases in magnitude at the expense of the high-

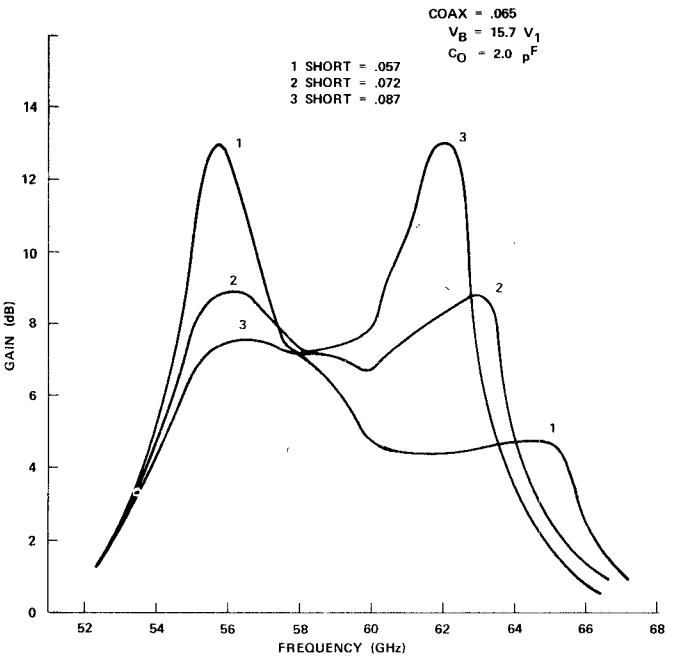

Fig. 10. Measured amplifier gain for a fixed coaxial length as a function of short position.

frequency peak, and vice versa. In fact, the calculation predicts that the gain increases monotonically with the short movement, eventually leading to oscillation at the peak gain frequency. This is exactly what has been observed with the actual amplifier. To obtain a quantitative comparison with measurements, the measured amplifier responses are shown in Fig. 10. When these curves are compared with those in Fig. 9, the agreement is quite satisfactory.

V. Conclusion

An approximate equivalent circuit model has been developed to aid in the design of IMPATT oscillators and amplifiers at V-band frequencies. Although the model has

been developed under some gross approximations, the calculated results have shown good agreement with experimental data using theoretical small-signal IMPATT characteristics. The circuit model developed is not restricted to IMPATT devices and should be applicable to similar waveguide circuits used for other solid-state devices.

Acknowledgment

The authors wish to thank R. S. Ying and E. M. Nakaji for providing the IMPATT devices, Dr. R. L. Bernick for providing Fig. 8, and Dr. T. A. Midford for many helpful discussions and encouragement during the course of this work.

References

[1] H. J. Kuno and D. L. English, "Nonlinear and large-signal characteristics of millimeter-wave IMPATT amplifiers," *IEEE Trans. Microwave Theory Tech.*, vol. MTT-210, pp. 703–706, Nov. 1973.
[2] ——, "Millimeter-wave IMPATT power amplifier/combiner," this issue, pp. 758–767.
[3] E. Yamashita and J. R. Baird, "Theory of a tunnel diode oscillator in a microwave structure," *Proc. IEEE*, vol. 54, April 1966.
[4] D. C. Hanson and J. E. Rowe, "Microwave circuit characteristics of bulk GaAs oscillators," *IEEE Trans. Electron Devices*, vol. ED-14, pp. 469–476, Sept. 1967.
[5] L. Infeld, "The impedance of a rectangular waveguide with a thin antenna," *Can. J. Res. Sect. A*, vol. 27A, pp. 109–129, July 1949.
[6] L. Lewin, "A contribution to the theory of probes in waveguides," *Inst. Elec. Eng. Mono. 259R*, pp. 109–116, Oct. 1957.
[7] R. L. Eisenhart and P. J. Kahn, "Theoretical and experimental analysis of a waveguide mounting structure," *IEEE Trans. Microwave Theory Tech.*, vol. MTT-19, pp. 706–719, August 1971.
[8] J. A. Bradshaw, "Scattering from a round metal post and gap," *IEEE Trans. Microwave Theory Tech.*, vol. MTT-21, pp. 313–322, May 1973.
[9] J. Schwinger and D. S. Saxon, *Discontinuities in Waveguides*. New York: Gordon and Breach Science Publishers, 1968.
[10] L. Lewin, *Advanced Theory of Waveguides*. London: Iliffe, 1951.
[11] R. E. Collin, *Field Theory of Guided Waves*. New York: McGraw-Hill, 1960.
[12] B. C. DeLoach, "A new microwave measurement technique to characterize diodes and an 800-GC cutoff frequency varactor at zero volt bias," *IEEE Trans. Microwave Theory Tech.*, vol. MTT-12, pp. 15–20, Jan. 1964.
[13] T. Misawa, "Negative resistance in p-n junction under avalanche breakdown conditions, Pts. I and II," *IEEE Trans. Electron Devices*, vol. ED-13, pp. 137–151, Jan. 1966.
[14] W. N. Grant, "Electron and hole ionization rates in epitaxial silicon at high electric fields," *Solid-State Electronics*, vol. 16, pp. 1189–1203, 1973.
[15] D. L. Scharfetter and H. K. Gummel, "Large signal analysis of silicon Read diode oscillator," *IEEE Trans. Electron Devices*, vol. ED-16, pp. 64–67, Jan. 1969.

Millimeter-Wave IMPATT Power Amplifier/Combiner

H. J. KUNO, SENIOR MEMBER, IEEE, AND DAVID L. ENGLISH, ASSOCIATE MEMBER, IEEE

Abstract—**The development of a two-stage millimeter-wave IMPATT power amplifier/combiner is described herein. The driver stage consists of a two-diode hybrid-coupled amplifier and the output stage consists of a four-diode combiner (a pair of hybrid-coupled amplifiers). An output power of 1 W was achieved with a 22-dB small-signal gain and a 6-GHz bandwidth in the 60-GHz range. Design considerations and experimental data are presented in detail.**

Introduction

THE APPLICATION of IMPATT devices in millimeter-wave systems has gained great importance in recent years. It has been demonstrated that IMPATT oscillators and amplifiers can be used effectively for millimeter-wave power generation and amplification [1]–[7]. It is of great interest to combine a number of diodes to achieve high output power. In the microwave frequency range various power combining approaches have been tried [8]–[14]. However, the same technique cannot readily be applied directly at millimeter-wave frequencies. This paper describes the development of a millimeter-wave IMPATT power amplifier/combiner with which a continuous-wave (CW) output power of 1 W was achieved with a 6-GHz small-signal bandwidth in the 60-GHz range.

The hybrid-coupled power amplifier/combiner, as applied to the millimeter-wave range, offers the following advantages over other approaches.

1) The power-impedance limitation of multidevice operation in a single cavity is removed. However, as will be shown in the next section, other considerations limit the number of devices which may be efficiently combined.

2) Since the hybrid coupler provides isolation between the individual amplifier cavities, instability problems associated with multidevice operation in a single cavity are minimized.

3) Ferrite circulators are not required if 90° hybrids are used.

4) Since hybrid couplers provide broad-band characteristics (BW = 10 GHz at 60 GHz), broad amplifier bandwidth can be achieved.

5) Since each amplifier cavity can be tuned individually, amplifiers can be well matched.

Manuscript received February 27, 1976; revised May 21, 1976. This work was supported in part by the Air Force Avionics Laboratory, Air Force Systems Command, U.S. Air Force, Wright-Patterson Air Force Base, OH.

The authors are with Hughes Aircraft Company, Torrance, CA.